Springer

KSME

Journal of Mechanical Science and Technology 24 (12) (2010) 2567~2575
www.springerlink.com/content/1738-494x
DOI 10.1007/s12206-010-0926-y

Examination of flame length for burning pulverized coal in laminar flow reactor †

Jae-Dong Kim[1], Gyu-Bo Kim[2], Young-June Chang[1], Ju-Hun Song[1] and Chung-Hwan Jeon[1,*]

[1]*School of Mechanical Engineering, Pusan National University, Busan, 609-735, Korea*
[2]*Pusan Clean Coal Center (PC[3]), Pusan National University, Busan, 609-735, Korea*

(Manuscript Received December 28, 2009; Revised March 31, 2010; Accepted August 6, 2010)

Abstract

Because there has been a recent increase in the use of low calorific coal compared to standard coal, it is crucial to control the char flame length governing the burning life-time of coal in a coal-fired utility boiler. The main objective of this study is to develop a simplified model that can theoretically predict the flame length for burning coal in a laboratory-scale entrained laminar flow reactor (LFR) system. The char burning behavior was experimentally observed when sub-bituminous pulverized coal was fed into the LFR under burning conditions similar to those in a real boiler: a heating rate of 1000 K/s, an oxygen molar fraction of 7.7 %, and reacting flue gas temperatures ranging from 1500 to 2000 K. By using the theoretical model developed in this study, the effect of particle size on the coal flame length was exclusively addressed. In this model, the effect of particle mass was eliminated to compare with the experimental result performed under a constant mass feeding of coal. Overall, the computed results for the coal flame length were in good agreement with the experimental data, particularly when the external oxygen diffusion effect was considered in the model.

Keywords: Char combustion; Coal flame length; Laminar flow reactor (LFR); Particle temperature; Diffusion; Particle size

1. Introduction

Coal has much greater reserves and lower costs than any other fossil fuel resource. It is therefore expected to remain an essential energy resource for the next several decades. As a matter of fact, coal has played a major role in electric power generation in the United States, China, India, and Korea through the years. Since the adoption of the Kyoto Protocol in 1997, alternatives to conventional coal combustion have been sought to increase the power generation efficiency and decrease pollutant emissions [1]. As examples, an integrated gasification combined cycle system [2-4] and super-critical pulverized coal combustion [5] are receiving a great deal of attention. However, the implementation and applicability of such emerging technologies to commercial systems requires an understanding of the combustion and gasification characteristics of coal [6]. A thorough understanding of such coal reaction processes could be gained through experimental study with either a laboratory-scale reactor or a pilot-scale boiler, both of which would require a specific facility and installation costs. Instead, some researchers have performed comprehensive 3-dimensional simulations in which coal reaction and dispersion are coupled with gaseous reacting flow with heat transfer. Again, this would be of great help in identifying the optimal reaction condition and would make it possible to obtain a better evaluation of the combustion characteristics of coal. For instance, a full-scale simulation of the particle-laden reacting flow occurring in a pulverized coal fired furnace was documented in the studies of Zhang et al. and Guo et al. [7, 8]. The computed results show the detailed trajectories of coal particles, along with the mass and temperature variations of the flue gas interacting with the particles burning in the furnace, indicating the strong dependence of these variations on the initial size of the coal particles. However, due to the inherent complexities such as the complicated geometry of the furnace and the coupling of a gas phase with a particle phase, it takes extensive time to obtain satisfactory results and is necessary to demonstrate the validity of a full-scale simulation against experimental results. A one-dimensional plug flow model has also been developed that involves a rigorous treatment of coal particle reactions but avoids the complexities of multi-dimensional fluid motion. Such a model is relatively inexpensive to operate and sufficiently general to permit its application to a wide range of coal reaction processes.

In contrast to such simulations, a zero-dimensional analysis emphasizes describing the combustion behavior of a single coal particle, where only the reaction and oxygen diffusion within a particle or to the surface are considered. Thus, the effects of a fluid motion, such as the turbulence and recircula-

† This paper was recommended for publication in revised form by Associate Editor Ohchae Kwon

* Corresponding author. Tel.: +82 51 510 3051, Fax.: +82 51 582 9818
E-mail address: chjeon@pusan.ac.kr

tion induced by the furnace geometry, and the boundary layer development around a particle, are neglected in this analysis. Due to its relative simplicity, it is quite suitable for evaluating the effect of combustion characteristics as a function of the coal property variation in a rapid manner. Stanmore et al. addressed the effect of the volatile contents on the formation of nitric oxide, which was predicted just from the simple model involving the combustion process for a single spherical coal particle [9, 10]. The char reaction occurs at a particle surface where volatile products are convected away and meet with oxygen to generate a volatile reaction. By assuming that both the char and volatile reactions occur right at a particle surface, Vamvuka et al. carried out a unique analysis describing the mass and heat transport processes around a single particle [11]. A system of ordinary differential equations describing oxygen content and energy conservation was solved using a combination of time integration and iterative solution techniques.

Following this approach, a more simplified analysis is provided in this paper, where the flame length for coal is predicted by solving just the mass balance equation. The accuracy of the prediction was evaluated by a comparison with experimental data observed in a laboratory-scale entrained laminar flow reactor (LFR) system [12].

2. Theoretical development

There are numerous reaction models where different levels of coal particle reactions are considered. Among them, the theory approached in this study originated from the char burning rate equation of Mitchell et al. [6].

The char burning rate, $r_c^{'}$, is defined as the mass loss per unit time, which can be expressed for a spherical particle. In some circumstances, the effect of oxygen diffusion on combustion should be evaluated rather than be neglected in the char burning rate. Thus, the rate considering oxygen diffusion effect is related via the effectiveness factor.

$$r_c^{'} = \frac{dm_c}{dt} = -\eta_e \cdot k_c^{`} \cdot (\frac{6}{\rho_c \cdot d_c}) \cdot m_c \cdot p_{O_2,\infty}, \quad (1)$$

where $k_c^{'}$ is a new kinetic constant [kg/ (m^2·s·Pa)] including pre-exponential factor and activation energy, which were experimentally determined as described in Appendix [13], ρ_c is the bulk density of a particle [kg/m^3], d_c is the diameter of a particle [m], m_c is the mass of a particle [kg] and $p_{O_2,\infty}$ is the partial ambient pressure of oxygen [Pa] [14].

In Eq. (1), η_e is the effectiveness factor for external diffusion, the diffusion to the particle surface. This effectiveness factor is a function of diffusion Thiele modulus at given conditions, which heavily depends on the temperature and particle size. The details of the relationship and relevant properties are further described in the reference [15]. Since the burning of coal is assumed to undergo a surface burning condition where a spherical particle burns mostly at its periphery, the diffusion within a particle, referred to as internal diffusion, was neglected. This condition is prevalent with a highly dense particle, within which a rigorous reaction occurs.

To convert Eq. (1) to a form expressed in terms of particle temperature, it is necessary to introduce a particle temperature gradient ($\alpha = -dT/dt$), with which it can be rearranged into:

$$\frac{dm_c}{m_c} = \eta_e \cdot k_c^{`} \cdot (\frac{6}{\rho_c \cdot d_c}) \cdot p_{O_2,\infty} \cdot \frac{dT}{\alpha} \quad . \quad (2)$$

Integrating both sides,

$$\int_{m_{c,0}}^{m_{c,t}} \frac{dm_c}{m_c} = \eta_e \cdot (\frac{6}{\rho_c \cdot d_c}) \cdot \frac{p_{O_2,\infty}}{\alpha} \times A \cdot \int_{T_0}^{T} \exp\left(-\frac{E_a}{R_u T}\right) dT, \quad (3)$$

where $m_{c,t}$ and $m_{c,0}$ are the mass of the particle at a certain burn-off time (t) and at the initial state, and T and T_0 are the temperature of the particle at a certain burn-off time (t) and at the initial state, respectively.

Eq. (3) can be rearranged into Eq. (4) by dividing one equation for a particle with a reference size (the smallest size) over another equation for a particle of a different size. Because the initial mass relevant to the coal feeding rate in the experiment and the final mass after the burn-off remain the same regardless of the different conditions, it is noted that the ratio term on the left side of Eq. (3) would be equal to one.

$$\int_{T_{1,0}}^{T_1} \exp\left(-\frac{E_a}{R_u T}\right) dT = \frac{\eta_{e,ref}}{\eta_{e,1}} \cdot \frac{d_{c,1}}{d_{c,ref}} \cdot \frac{\alpha_1}{\alpha_{ref}} \cdot \int_{T_{ref,0}}^{T_{ref}} \exp\left(-\frac{E_a}{R_u T}\right) dT. \quad (4)$$

From this formula, a primary variable, the burn-off temperature of a particle (T_1), was numerically solved using the iterative method available in the non-linear solver of a commercial mathematical software. During this determination, three temperatures, including $T_{ref,0}$, T_{ref}, and $T_{1,0}$, and the temperature gradients (α_1, α_{ref}), were known in advance from the measurement of the particle temperature variation for particles with different sizes. The flame length was then obtained by substituting the burn-off temperature (T_1) into a spatial variation curve for particle temperature already fitted to the measured data for a coal particle. As implied in the equation, a burn-off temperature and its resultant flame length are significantly affected by the terms placed in front of the integral on the right side denoted as the total coefficient (C_t).

The coefficient is described in terms of three different effects: the inverse of the effectiveness factor ratio, the particle size ratio, and the particle temperature gradient ratio, all of which are normalized with respect to a reference condition (a particle of the lowest size in this case). This relation will be used to illustrate how these three parameters would significantly affect the coal flame length in response to the particle

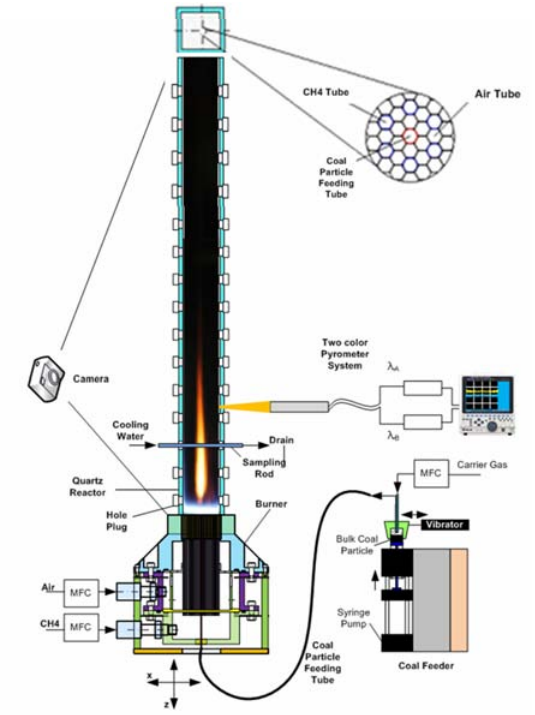

Fig. 1. Schematic diagram of laminar flow reactor system equipped with optical diagnostics.

size change described in the next section.

$$C_t = \frac{\eta_{e,ref}}{\eta_{e,1}} \cdot \frac{d_{c,1}}{d_{c,ref}} \cdot \frac{\alpha_1}{\alpha_{ref}} = \left(\frac{1}{\eta_{e,N}}\right) \cdot d_{c,N} \cdot \alpha_N , \quad (5)$$

where $\eta_{e,N}$ is the normalized effectiveness factor, $d_{c,N}$ is the normalized particle size, and α_N is the normalized particle temperature gradient.

3. Experimental setup

3.1 Experimental apparatus

The experiments were conducted in a laminar flow reactor (LFR) system designed and fabricated by the Pusan Clean Coal Center (PC^3) at Pusan National University. A schematic diagram of the experimental apparatus is shown in Fig. 1 [12].

The apparatus is based on the laminar flow methane-air flame burner used by Kramlich et al. [16, 17] for studying the combustion kinetics of a coal particle. The current burner is made up of a hexagonal honeycomb in which stainless tubes are distributed and inserted to make a bundle of flat flame to initiate a series of combustion processes for a single coal particle and ensure a uniform temperature distribution across the burner. The central tubes are used as a passage to supply methane (CH_4), whereas the six neighboring tubes are for an oxidizer such as air. The coal particles delivered by a carrier gas (N_2) are injected along the centerline of the reactor at a constant feeding rate controlled by a feeding system built in-house and equipped with a vibrator and pneumatic syringe.

Table 1. Specifications of experimental apparatus.

Burner dimensions (mm)	
Inner burner	27 × 27
Outer burner	70
Weight (kg)	5
Max. gas temp. (K)	2000
Max. heating rate (K/s)	1000
Flame type	Laminar diffusion flame
Coal tube diameter (mm)	0.8 (I.D.)
Gas / fuel tube diameter (mm)	0.8 (I.D.)

Table 2. Properties of coal used in this study.

Coal	Roto-Middle
Proximate analysis (dry basis) (wt.%)	
Moisture	12.6
Volatile matter	46.6
Fixed carbon	38.0
Ash	2.8
Ultimate analysis (dry basis) (wt.%)	
Carbon	69.7
Hydrogen	5.5
Nitrogen	0.76
Sulfur	0.04
Oxygen	20.86
Ash	3.14
Kinetic parameters	
Pre-exponential factor (kg/m^2-s-Pa)	91.2
Activation energy (J/mol)	7.0×10^4

The transparent quartz walls mounted on top of the reactor allow the natural light emitted from the burning coal particles to be observed by optical diagnostics, including a two-color pyrometer and video camera [18].

Table 1 lists the detailed specifications of the LFR, such as its dimensions and weight. The LFR has a great advantage over other types of reactors used for coal combustion research in that it can provide a combustion environment analogous to a real utility boiler furnace in terms of the maximum gas temperature and heating rate.

3.2 Coal sample preparation

The coal sample used in this experiment was Roto-Middle coal imported from Indonesia that is widely used as pulverized coal in coal-fired power plants in South Korea. The as-received raw coal was first ground in a manually operated pulverizer and then sieved repeatedly with vibration; the coal thus obtained were classified into three different size fractions: 32-45, 75-90, and 150-180 μm.

A proximate analytical result was obtained using a thermogravimetric analyzer (SDT Q600) according to ASTM procedures [19], while an ultimate analysis was made through a commercial device (Leco-TruSpec Micro CHNS). The chemical characteristics of the coal and the kinetic parameters ob-

Table 3. Experimental conditions.

Gas flow conditions	
CH_4 (sccm)	380
Air (slm)	6.02
Carrier N_2 (sccm)	30
Coal burning conditions	
Equivalence ratio	0.613
Oxygen molar fraction (%)	7.67
Coal feeding rate (g/h)	0.1
Gas temperature (K)	1500–2000

tained from the experimental method described in Eqs. (9) and (10) in Appendix are presented in Table 2. Based on the H/C and O/C ratios obtained from the ultimate analysis, the coal sample was a typical sub-bituminous coal that contained a relatively high amount of volatile matter compared to its fixed carbon content.

3.3 Experimental conditions and techniques

The flow conditions for the combustible gases selected for this test are listed in Table 3. The primary gases supplied were air as an oxidizer and methane as a fuel, with an equivalence ratio of approximately 0.61, to produce a number of laminar diffusion flamelets to be used for initiating coal burning processes. It should be noted that the formation of such flames results in the cleanest flat flame without soot formation, where the temperature of the post flame gases would be evenly distributed across the burner and would be as close as possible to an adiabatic flame temperature due to the minimization of heat loss. At these flue gas conditions, where the coal was injected and was about to burn, an oxygen molar condition fraction of 7.67 and gas temperatures varying from 1500 up to 2000 K were easily accomplished. As mentioned before, such conditions would be analogous to the combustion environment of a utility boiler furnace in terms of the gas temperature and available oxygen molar fraction.

By varying the displacement rate of the syringe pump in the coal feeding system according to the different sizes of particles, the coal feeding was maintained at a fixed mass flow rate of 0.1 g/h. This precise control isolated the effect of the particle size on the char burning behavior from the combined effect of particle mass and size that inevitably occurred as the particle size was changed in the feeding system of the LFR. The coal flame length and onset position for char burning were observed and recorded with a CCD camera under steady state operation, after a 10 minute warm-up from the start of the experiment. The individual image was the trace of coal flame captured in the CCD camera during a long exposure time of approximately one second. The coal flame length was determined based on an average of 15 to 20 images for the three different sizes of particles by a proprietary image processing technique. For the statistical quantification of the length, a standard deviation of flame lengths was introduced for particles of different sizes. From its comparison with the length of an average coal flame, the measured coal flame length was found to be statistically significant, which is quite acceptable for a further analysis.

Optical measurements on the surface temperature of burning coal particles have been made in numerous studies, including those of Howard et al. [20], Ayling et al. [21], Niksa et al. [18], Mitchell et al. [22], and Levendis et al. [23, 24]. In particular, the pyrometry technique of using the ratio of two wavelengths attempted by Ronald [25] was employed in this study. As seen in Fig. 1, a two-color pyrometer system, a mainly non-instructive diagnostic tool for surface temperature, was set up to yield the local temperature variation of burning particles. A collecting lens was used to focus pyrometric signals emitted from the burning particle at a specific height and then a detector system with two wavelength channels where interference filters, a photo multiplier tube (PMT) and a data acquisition system (Memory Hi-corder) were mounted. The emitted signals were detected through two bandwidth filters with center wavelengths of 650 nm and 700 nm with a full width half maximum (FWHM) of 10 nm. Experimental uncertainty may be reduced by selecting two filters with center wavelength much wider than ones currently used in this experiment. However, the regression result to be seen in Fig. 2 shows that a relation of intensity ratio with an inverse of particle temperature is fairly linear within a reasonable deviation. As long as the linearity is satisfied, it indicates that current selection of two wavelengths (650 and 700 nm) is yet applicable to be further used for the determination of a particle temperature.

To determine temperature, assuming that the emissivity is not a function of the wavelength, the ratio of the two signal intensities is directly related to the temperature via Planck's radiation law, as expressed in:

$$T = \frac{C_2\left(\frac{1}{\lambda_B} - \frac{1}{\lambda_A}\right)}{\ln\frac{I_A}{I_B} - \ln C}, \tag{6}$$

where C_2 is Planck's second radiation constant with a value equal to 1.44 cm·K, and $C = \frac{\eta_{L,A}\eta_{D,A}\lambda_B^5\Delta\lambda_A}{\eta_{L,B}\eta_{D,B}\lambda_A^5\Delta\lambda_B}$ is a characteristic value of the optical components, including the detector and optical filter. I_i represents the measured signal intensities, $\eta_{L,i}$ are the efficiencies for carrying light to the detectors, $\eta_{D,i}$ are the detector efficiencies at each wavelength, λ_i are the wavelengths for the two channels, and $\Delta\lambda_i$ are the bandwidths used for the detection. While the efficiencies of each component are difficult to measure, the mean characteristic value of optical components, C, was statistically determined by the calibration process, which is to be described in detail.

The calibration of an in-house two color pyrometer was performed by a commercially available pyrometer integrated with

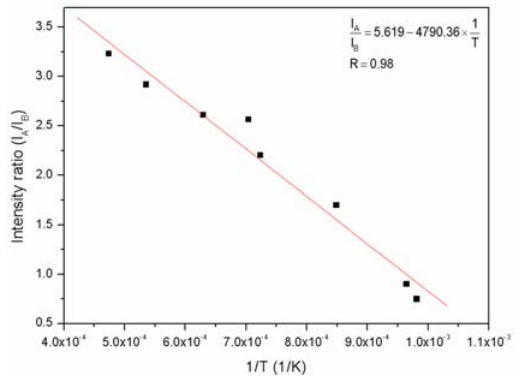

Fig. 2. The calibration result of the two-color pyrometer where the intensity ratio of two signals is linearly related with the inverse of temperature.

a luminescent tungsten lamp. Fig. 2 presents the calibration result of the two-color pyrometer where the previous value, approximately equal to 0.76, was obtained for a mean characteristic value. More specifically, the corresponding value of the intensity ratio detected at different temperatures is substituted in Eq. (6) to produce a distribution of characteristic values where its mean value is determined.

In Fig. 2, the formula fitted over raw data of the intensity ratio against the inverse of temperature is seen, which is eventually used to determine the burning particle temperature.

The commercial pyrometer used to calibrate was reported to have an error level of ± 0.4%, which considers any measurement uncertainties. Also, the error level for the curve fitting made for the intensity ratio against an inverse of temperature was found to be ± 2% as inferred from Fig. 2. After every error source is considered, total error level increased to ± 2% (about ± 40K temperature deviation) as indicated in the Fig. 4. This is marginally acceptable because it is still less than the magnitude in changes of particle temperature in a response to size change.

4. Results and discussion

4.1 Flame structure and length measurement

Fig. 3 shows optical images of coal flame structures burning in the LFR system under the same coal feeding rate as a function of particle size. In general, the combustion processes for coal particles involve drying, devolatilization, and char combustion. As a coal particle is rapidly heated by the high temperature oxidizing condition of a blue flat flame, it starts releasing volatile matters in a gas-phase. The particle temperature at such a region of devolatilization was much higher than that of char combustion, because a yellowish luminescent flame of higher intensity was predominantly observed as the volatile matter burned near the particle. The char combustion region occupies the slowest and thus largest part of the entire process. In other words, the char burning time is much higher than that for any other process because the solid carbon content of the particle reacts heterogeneously with the oxygen in the air.

Table 4. Summary of measured flame length and onset position of char burning for different coals.

Coal size (μm)	32-45	75-90	150-180
Onset of char burning (mm)	12.5	40	75
Average flame length (mm)	74.8	124	168.3
Normalized standard deviation	0.033	0.07	0.096

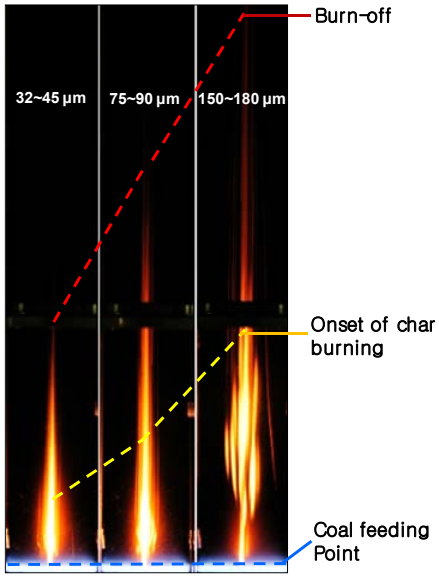

Fig. 3. Coal flame structures with drying, devolatilization, and char burning regime for three different sizes of coals burning in entrained laminar flow reactor system.

The flame length of the coal referenced from the injected position was measured by using the appropriate image processing from the natural luminosity in the optical image. The experimental data obtained is listed in Table 4. [12]. The flame lengths of coal burning for the three different particle sizes were 74.8, 124, and 168.3 mm, where char burning was initiated at 12.5, 40, and 75 mm, respectively. As the particle size increased, the coal flame length as well as the onset position of the char burning was likely to increase.

4.2 Particle temperature measurement

Under the constant coal feeding rate and oxygen concentration, particle temperature measurements were made at various reactor heights for a given particle size. As seen in Eq. (6), the particle temperature was determined using the peak intensities of the pyrometer signals at two wavelengths.

Fig. 4 presents the spatial dependence of the particle temperature evaluated for coal particles with three sizes. The results show that the combustion of 32–45 μm coal particles produced a particle temperature of roughly 1977 K at a beginning height of 12.5 mm, which was used for $T_{ref,0}$ in Eq. (4). The combustion of this particle was completed with a burn-off temperature of 1674 K at a height of 75 mm, which was used for T_{ref} in Eq. (4). For coal particles with larger sizes of 75–

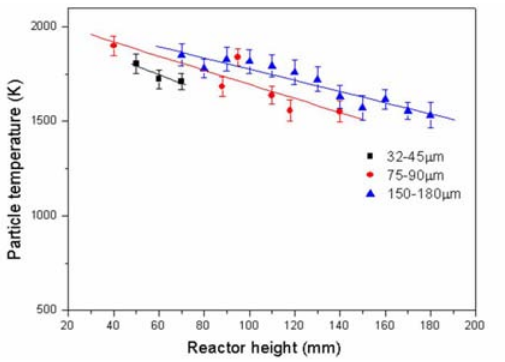

Fig. 4. Axial variation in measured particle temperature for three different sizes of coal.

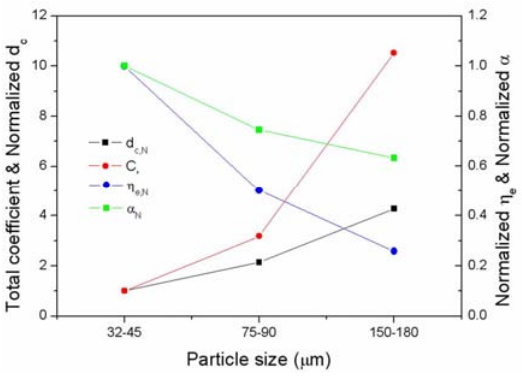

Fig. 5. Variation in total coefficient (C_t) with three particle sizes of coal indicating contributions from three effects, i.e., particle size ($d_{c,N}$), particle temperature gradient (α_N), and effectiveness factor ($\eta_{e,N}$), all of which are normalized with respect to reference condition (a particle of the lowest size in this case).

90 and 150–180 μm, the char burning launched at lower temperatures of approximately 1903 K and 1858 K, which corresponded to heights of 40 and 75 mm, respectively. These temperature magnitudes at the onset position of char combustion were determined by a linear regression formula using the raw data of the particle temperature against the reactor height and were used for $T_{1,0}$ in Eq. (4).

The figure also shows the significant dependence of both the particle temperature and axial gradient of the temperature on the particle size. As the particle size increased, the overall particle temperature increased over the entire distance that the coal burned. The radiant intensity of a burning particle was directly proportional to the projected surface area of the particle, indicating the size effect on the elevation of particle temperature. However, as discussed previously, the particle temperature was obtained, not from the magnitudes of the intensities at the two wavelengths, but from the relative intensity ratio for 650 nm and 700 nm. Therefore, the effect of the surface area and its resultant size may be cancelled out, so as not to be a primary factor for the increase in the particle temperature. Instead, in the case of the combustion of a group of particles, the char burning rate increased significantly with an increase in particle size where the heat generation of the larger particles was much greater than that of small particles under the same heat loss condition. The latter situation could explain the probability of the higher particle temperature observed with larger coal particles in the figure.

Fig. 5 presents the variation of normalized particle size ($d_{c,N}$), particle temperature gradient (α_N), and effectiveness factor ($\eta_{e,N}$) with particle sizes, where the values of these parameters for the two sizes of larger particles were normalized with respect to one of the particle of the lowest size (32–45 μm).

The results clearly illustrate how differently these parameters would affect the magnitude of the total coefficient (C_t) in determining a coal flame length in response to particle size change, as expressed by Eq. (5). As the particle size increases, the ratio of the axial gradient of particle temperature, α_N, becomes smaller, indicating a small change in the particle's temperature as it travels upward. However, as the particle size increases, the ratio of the effectiveness factor for external diffusion, $\eta_{e,N}$, decreases more compared with the change in α_N, as seen in the figure. The effectiveness factor that is a function of the Thiele modulus represents the degree of external diffusion. A factor equal to one means that no diffusion limitation is involved in the coal burning where the oxygen in the surrounding air is fully available at the particle surface. As the factor, however, goes to zero, the diffusion becomes a controlling process in coal combustion where oxygen is limited at the particle surface. As seen in the definition of the Thiele modulus available in Ref. [15], the modulus and thus the effectiveness factor have a strong dependence on the particle temperature and particle size. As the particle size increased, the particle was likely to attain an elevated temperature; consequently, the effectiveness factor dropped more rapidly, owing to the two combined effects than owing to the particle temperature gradient. It should be noted that there is a mild variation in the particle size ratio, $d_{c,N}$, with a size change as compared to the above two contributing parameters. Thus, the total coefficients for two large-sized particles increased mainly due to decreased values of $\eta_{e,N}$ as the particle size increased. This indicates that the external diffusion was more effective at changing the total coefficient and the resultant coal flame length than the particle temperature, even though the particle temperature indirectly produced a favorable condition for external diffusion. The increase in the total coefficient led to slowing down of the combustion rate and hence retarding of the coal flame length, which again indicated the greater importance of external diffusion in the char combustion processes.

4.3 Flame length prediction

Fig. 6 displays a comparison of the computed flame lengths and experimental lengths determined from optical images. As has been discussed, the coal flame lengths for 75-90 and 150-180 μm particles could be numerically predicted with respect to that of 32-45 μm particles using the theoretical model expressed in Eq. (4). The particle temperature variation, ratio of the effectiveness factors for external diffusion, ratio of the

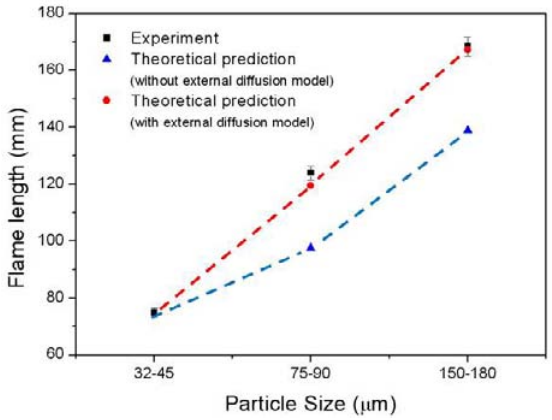

Fig. 6. Comparison between coal flame lengths obtained by theoretical predictions (with or without diffusion considered in the model) and experimental data for coal particles with three different sizes.

temperature gradient, and onset temperature of char burning were experimentally measured for incorporation in the formula. As a result of the prediction with a consideration of external diffusion, the burn-off temperatures of 75–90 and 150–180 μm coal particles were 1616.13 and 1575.96 K, which corresponded to heights of 119.5 and 167.1 mm, respectively. The burn-off temperatures of 75-90 and 150–180 μm coal particles predicted without considering the external diffusion effect were 1695.44 and 1662.71 K, which corresponded to heights of 97.59 and 138.84 mm, respectively. When comparing the former ones with the measured ones in the figure or those summarized in Table 4, the difference between them is not discernible, indicating the greater predictability of the model, particularly with external diffusion included.

The result computed with the external diffusion effect is far closer to the experimental one than that without considering the external diffusion effect. This comparison may indicate that the model that includes the concept of external diffusion would be sufficiently accurate to predict the overall combustion behavior of coal, such as the burning length, in a less time-consuming manner, although many complicated combustion processes were approximated to a greater extent.

In particular, an analysis with the simplified model developed in this study would be quite useful for an application where it is necessary to rapidly acquire information on changes in the burning behavior with different coals before a full test is made of how differently a coal-fired utility boiler responds to the coal. Nonetheless, this model should still be further modified to properly describe other aspects of coal combustion, including the changes in particle velocity and gas temperature surrounding the coal flame, the evolution of internal pore diffusion, and so on.

5. Conclusions

(1) To predict the flame length for burning coal in a laboratory-scale entrained laminar flow reactor system, a simplified model of a single particle was developed; in this model, it was necessary to determine the particle temperature across the flame from an experiment.

(2) In the model evaluation, the effect of the particle size on the coal burning behavior was exclusively addressed because the model readily decouples the effect of particle mass, which could otherwise affect the coal combustion.

(3) The computational accuracy of the model for predicting the coal flame length was greatly improved when the external diffusion effect was considered in the model.

(4) This result indicates that as the particle size increases, the external diffusion to slow down the burning of coal char becomes dominant. Therefore, the period for which the coal flame burns is extended more by external diffusion than by other parameters such as particle temperature and size.

Acknowledgment

This work was supported by the Human Resources Development of the Korea Institute of Energy Technology Evaluation and Planning(KETEP) grant funded by the Korea government Ministry of Knowledge Economy *(No. 2007-P-EP-H-ME-03-0000).*

References

[1] J. J. Murphy and C. R. Shaddix, Combustion kinetics of coal chars in oxygen-enriched environments, *Combustion and Flame,* 144 (2006) 710-729.

[2] L. Jiang, R. Lin, H. Jin, R. Cai and Z. Liu, Study on thermodynamic characteristic and optimization of steam cycle system in IGCC, *Energy Conversion and Management,* 43 (2002) 1339-1348.

[3] O. G. Guillermo, P. Douglas, E. Croiset and L. Zheng, Technoeconomic evaluation of IGCC power plants for CO_2 avoidance, *Energy Conversion and Management,* 47 (2006) 2250-2259.

[4] S. Rezvano, Y. Huang, M. W. David, N. Hewitt and J. D. Mondel, Comparative assessment of coal fired IGCC systems with CO_2 capture using physical absorption, membrane reactors and chemical looping, *Fuel,* 88 (2009) 2463-2472.

[5] S. Rezvani, Y. Huang, M. W. David, N. Hewitt and Y. Wang, Comparative assessment of sub-critical versus advanced super-critical oxyfuel fired PF boilers with CO_2 sequestration facilities, *Fuel,* 86 (2007) 2134-2143.

[6] R. E. Mitchell, L. Ma and B. J. Kim, On the burning behavior of pulverized coal chars, *Combustion and Flame,* 151 (2007) 426-436.

[7] J. Zhang and L. Zhou, Particle behaviors in a pulverized coal-fired sudden-expansion combustor with coaxial jets, *Fuel,* 80 (2001) 289-299.

[8] Y. C. Guo, C. K. Chan and K. S. Lau, Numerical studies of pulverized coal combustion in a tubular coal combustor with slanted oxygen jet, *Fuel,* 82 (2008) 893-907.

[9] S. P. Visona and B. R. Stanmore, Modeling NOx release

from a single coal particle I: Formation of NO from volatile nitrogen, *Combustion and Flame,* 105 (1996) 92-103.

[10] S. P. Visona and B. R. Stanmore, Modeling NO_x release from a single coal particle II: Formation of NO from char-nitrogen, *Combustion and Flame*, 106 (1996) 207-218.

[11] D. Vamvuka and E. T. Woodburn, A model of the combustion of a single small coal particle using kinetic parameters based on themogravimetric analysis, *Int. J. Energy Res.,* 22 (1998) 657-670.

[12] C. H. Jeon, Y. G. Kim, J. D. Kim, G. B. Kim and J. H. Song, An experimental investigation on combustion characteristic of a pulverized low calorific sub-bituminous coal with varying size by a LFR system, *KSME Journal,* B 34 3 (2009), in press.

[13] R. E. Mitchell, Experimentally determined overall burning rates of coal chars, *Combust. Sci. and Tech*., 53 (1987) 165-186.

[14] I. W. Smith, The combustion rates of coal chars: A review, *19th Symposium on Combustion,* (1982) 1045-1065.

[15] J. H. Song, C. H. Jeon and A. L. Boehman, Impacts of oxygen diffusion on the combustion rate of in-bed soot particles, *Energy & Fuels* (2010), available online.

[16] J. C. Kramlich, W. R. Seeker and S. G. Samuelsen, Observations of chemical effects accompanying pulverized coal thermal decomposition, *Fuel,* 67 (1988) 1182-1189.

[17] M. T. Brink, A fundamental investigation of the flame kinetics of coal pyrite, *Fuel,* 5 (8) (1996) 945-951.

[18] D. A. Tichenor, R. E. Mitchell, K. R. Hencken and S. Niksa, Simultaneous in situ measurement of the size, temperature, and velocity of particles in a combustion environment, *Twentieth Symposium (International) on Combustion / The Combustion Institute* (1984) 1213-1221.

[19] J. P. Mathews, P. G. Hatcher and A. W. Scaroni, Particle size dependence of coal volatile matter: Is there a non-maceral-related effect?, *Fuel,* 76 (4) (1997) 359-362.

[20] J. B. Howard and R. H. Essenhigh, Combustion mechanisms in pulverized coal flames, *Combustion and Flame,* 10 (1996) 92-93.

[21] A. B. Ayling and I. W. Smith, Measured temperatures of burning pulverized-fuel particles, and the nature of the primary product, *Combustion and Flame*, 18 (1978) 173.

[22]R. E. Mitchell, W. J. Mclean, On the temperature and reaction rate of the burning pulverized coal, *Proc. Combust. Instit.*, 19 (1982) 1113.

[23] Y. A. Levendis, K. R. Estrada and H. C. Hottel, Development of multi color pyrometers to monitor the transient response of burning carbonaceous particles, *Rev. Sci. Instit.*, 63 (7) (1992) 3608.

[24] P. A. Bejarano and Y. A. Levendis, Single-coal-particle combustion in O_2/N_2 and O_2/CO_2 environments, *Combustion and Flame* 153 (2008) 207-287.

[25] A. D. Ronald, Determination of complete temperature profiles of singly burning pulverized fuel particles, MIT, Master Thesis (1979) 24-27.

[26] B. H. Lee, J. H. Song, K. T. Kang, Y. J. Chang and C. H. Jeon, Determination of char oxidation rates with different analytical methods, *KSME Journal*., B 33 11 (2009) 876-885.

[27] F. Veglio, M. Trifoni, F. Pagnaelli and L. Toro, Shrinking core model with variable activation energy: A kinetic model of magneticferrous ore leaching with sulphuric acid and lactose, *Hydrometallurgy,* 60 (2001) 167-179.

[28] A. Szubert, L. Michal and S. Zygmunt, Application of shrinking core model to bioleaching of black shale particles, *Physicochemical Problems of Mineral Processing,* 40 (2006) 211-225.

Appendix

A. Determination of kinetic parameters

The carbon consumption rate, $r_{c,unit\,area}^{`}$, which is equal to the char burning rate per unit area, was experimentally determined in the same LFR apparatus from the change in a measured particle's radius, from its initial value of r_0 to r_t during a burn-off process [26-28]. It can be expressed by:

$$r_{c,unit\,area}^{'} = \left(\frac{\rho_c}{t}\right)(r_0 - r_t)\,, \tag{A.1}$$

where r_0 and r_t are the initial particle radius and the particle radius after a certain burn-off time, t, respectively, and ρ_c is the bulk density of a particle.

In this determination of $r_{c,unit\,area}^{`}$, the mean particle radius is required and obtained statistically from the size distribution measured with a micrograph from a scanning electron microscope (SEM). Because $r_{c,unit\,area}^{`}$ is now known, a new kinetic constant, $k_c^{'}$, can be easily calculated at different particle temperatures using the following equation, which is slightly modified from Eq. (1).

$$r_{c,unit\,area}^{'} = -\eta_e \cdot k_c^{'} \cdot p_{O_2,\infty} \tag{A.2}$$

The kinetic parameters (A, E_a) are finally determined from the Arrhenius plot of the kinetic constant against an inverse particle temperature, where a linear regression to fit the kinetic constant data was taken. The resultant values are listed as one of the properties of coal in Table 2.

There are other kinetic analyses to extract kinetic parameters which differ in the manner the char burning rate is obtained. Those have their own merits and limitations due to an inherent assumption derived for the corresponding rate expression as discussed in Ref. [26]. Recognizing the fact that the rate expression in Eq. (1) was developed under the assumption of a surface burning, the current kinetics method obtained exclusively from the radius change is a better means among others since its validity is also restricted to the surface burning condition. There exist other limitations of the method: this may not be applicable for the reaction conditions which are not approximated with a single-step global reaction and the first-order dependence of its rate on the oxygen content.

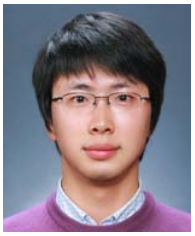

Jae-Dong Kim received his B.S. in Mechanical Engineering from Pusan National University in 2009. He is now an M.S. candidate in Mechanical Engineering at Pusan National University. His research interests include optical diagnostic techniques examining the combustion behavior of single coal particle.

Gyu-Bo Kim received his B.S. in Mechanical Engineering from Pukyong National University in 2000. He then received his Ph. D degree from Pusan National University in 2008. Dr. Kim is currently a research professor at Pusan Clean Coal Center in Pusan National University.

Young-June Chang received his B.S. and M.S degrees from Pusan National University in 1975 and 1977, respectively. He then received the Ph.D. from Tokyo Institute of Technology in 1986. Dr. Chang is currently a professor at the school of mechanical engineering in Pusan National University.

Ju-Hun Song received his B.S. and M.S. in Mechanical Engineering from Seoul National University in 1991 and 1996, respectively. He then received his Ph.D. from Pennsylvania State University, USA in 2005. Dr. Song is currently an assistant professor at the school of mechanical engineering at Pusan National University.

Chung-Hwan Jeon received his B.S. (1985), M.S. (1987) and Ph.D. (1994) degrees from Pusan National University. Dr. Jeon is currently an associate professor at the school of mechanical engineering at Pusan National University, and is currently serving as a director of Pusan Clean Coal Center.